Papers

The text of a proposed design method for rigid walls constructed in-situ in overconsolidated clay was published in the issue of Ground Engineering Volume 22 Number 8. Unfortunately due to space restrictions the diagrams were published at a size which made them difficult to read. They have now been republished below together with a summary of the accompanying text and a worked example which illustrates the new method of calculation, and references and the conclusions to Part I dealing with the construction phase. Design calculations pertinent to the long term equilibrium of such walls will be offered in Part II to be published in the next issue.

The design of in-situ walls retaining overconsolidated clay: Part I Short term behaviour

M D Bolton[1] W Powrie[2] & I F Symons[3]

Introduction

A method is set out by which designers can check both the safety and serviceability of relatively stiff reinforced concrete retaining walls constructed in-situ in overconsolidated clay.

Conventional design calculations are of the limit equilibrium type, being based on the assumption of 'fixed-earth' or 'free-earth' support conditions illustrated in

Figure 1. Current guidance in CIRIA Report 104 (Padfield and Mair 1984) is that the fixed earth support calculation is relevant only to unpropped walls and that free earth support conditions are more realistic for stiff propped walls which approach a failure condition by rotation about the prop position. A lumped factor of safety is used in conjunction with limiting 'active' and 'passive' earth pressures. The resulting design depends not only on the magnitude of the factor of safety adopted but also on the particular way in which it is introduced into the calculations. No explicit information is provided on the likely displacements in service.

The proposed method proceeds in three steps. The first step is simply to calculate the soil strength which must be mobilised to hold the proposed structure in equilibrium, using conventional stress distributions. The second step is to use stress-strain data to deduce the average soil shear strain which would be needed to mobilise this soil strength. In a third step, this average shear strain will be used to attribute strains to the various active and passive zones in a manner consistent with rigid body wall movements, which can then be deduced.

In situ stresses

Ground conditions before construction of the wall will vary from site to site, the in situ lateral earth pressure coefficient $K_o = \sigma'_h/\sigma'_v$ being a function of the ground water conditions, the effective stress history and the current stress state of the soil. Ancient clays which have been overconsolidated by the removal of overburden are usually found to have K_o greater than 2 in the region affected by wall construction. Installation of the wall will undoubtedly alter the initial stress state but the exact effect will depend on the details of the construction technique. For diaphragm walls, excavation under bentonite is likely to reduce the lateral stresses at the boundaries of the panel to the hydrostatic pressure of the bentonite. For bored pile walls the magnitude of the reduction in stress is likely to depend on the sequence of pile construction and whether casing is used to support the ground prior to pouring of the concrete.

As the wall is cast, further changes will occur depending on the relative rates of pouring and setting of the concrete. An upper limit on the boundary lateral total stress at this stage would be the hydrostatic pressure of wet concrete, corresponding approximately to $K_o = 1$. This simple condition also served as a convenient starting point for centrifuge model tests, used to investigate the validity of the new calculation methods, and it will be used in this paper as the datum for design calculations of plane strain deformations following wall construction.

Fig. 1 Fixed and free earth support conditions (after Padfield and Mair, 1984).

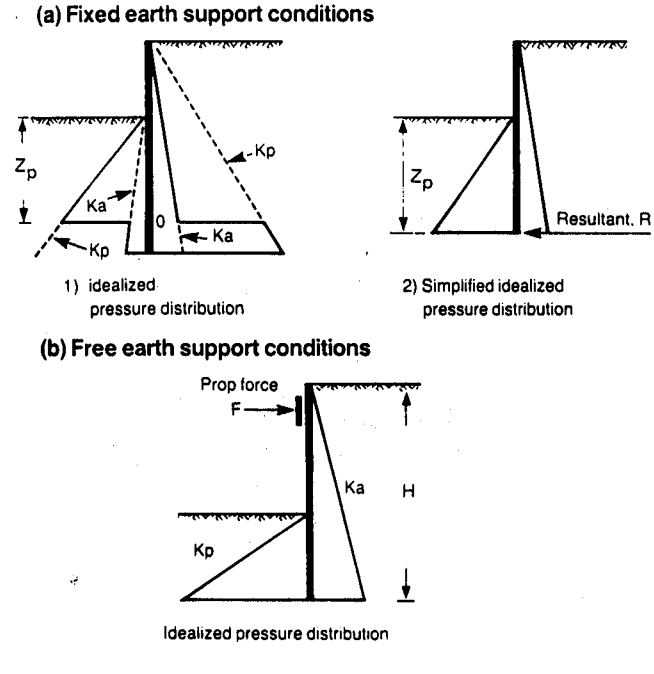

Stability on excavation

The undrained stability of the wall is most easily assessed using a lower-bound approach based on permissible stress fields, assuming a uniform undrained strength c_u. It is necessary to take into account the possible depth h_c of a vertical tension crack on the retained side. ***Figure 2*** shows idealised lateral pressure diagrams appropriate to soil of unit weight $\bar{\gamma}$ which cracks against a collapsing frictionless wall, the cracks either remaining dry or filling with water as the remainder of the clay shears in an undrained fashion. Wall height and pivot position can be selected so that equations of force and moment equilibrium can simultaneously be satisfied.

With dry cracks, it was found that the theoretical point of pivot was never more than 2.5% of the total height of the wall up from the base. A simplified fixed-earth support calculation ***(Figure 1a(2))*** would therefore have been perfectly adequate, with only a 2.5% height addition for toe support. With water filling cracks however, the pivot moved up to about 8% of the height. In that case, a fixed earth analysis of the upper 92% of the wall, taking moments about a point 4% up from the bottom where the equivalent toe-force could be said to act, would prove sufficiently accurate if moderate variations of soil strength with depth had to be accounted for.

Figure 3 gives non-dimensional plots of the undrained shear strength $^c/_{\bar{\gamma}h}$ required to achieve equilibrium for frictionless, rigid walls with different ratios of the penetration depth d to retained height h in clay of uniform strength. A typical excavation in overconsolidated clay might have $^{c_u}/_{\bar{\gamma}h} \simeq 1$, which apparently demands no embedment of the wall below excavation level if water can be excluded from tension cracks. A penetration ratio of about 0.6 for typical $\bar{\gamma}/\gamma_w$ of 2 would,

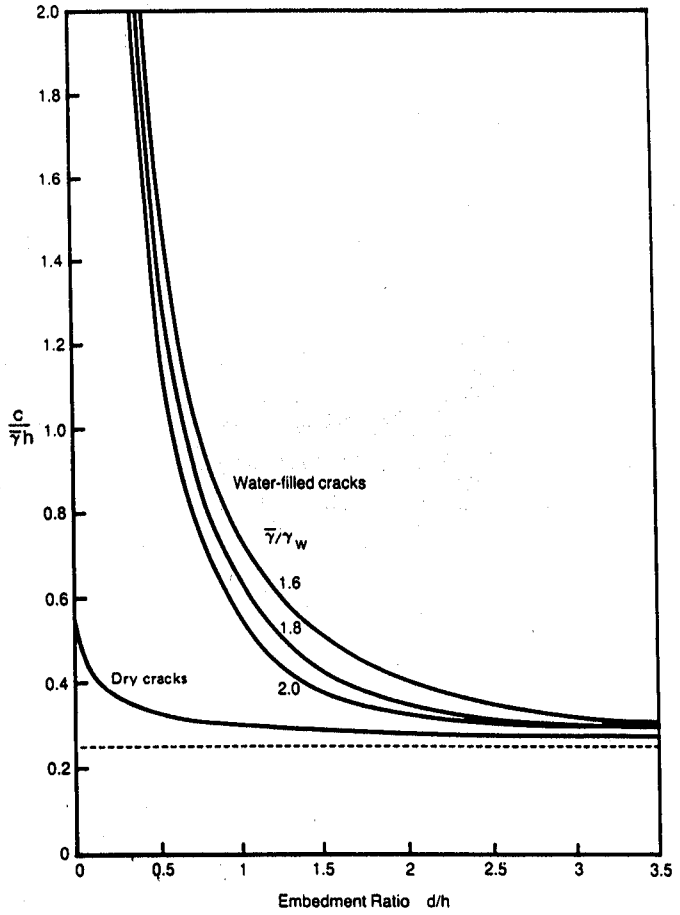

Fig. 3 Mobilised shear strength $\left(\frac{c}{\bar{\gamma}h}\right)$ ***as a function of embedment ratio*** $\frac{d}{h}$ ***for unpropped cantilever walls.***

however, be required just to prevent collapse if water could fill cracks.

Figure 4 shows the rather simpler pressure conditions which can be assumed for rigid walls propped at the top in clay of uniform strength. Their solution is more straightforward since the required penetration can be found directly from moment equilibrium about the prop, while horizontal equilibrium separately dictates the prop force. ***Figure 5a*** shows that the impact on wall stability of water in cracks on the retained side is somewhat less than with free walls. Prop forces, non-dimensionalised by dividing them by the equivalent 'hydrostatic' thrust of the retained face, are shown in ***Figure 5b:*** the effect of a water-filled crack beneath the prop is to more than double the required prop force.

Wall friction, and an increase in undrained strength with depth, can be accounted for if desired. However, the use of ***Figure 3*** or ***5*** in conjunction with the average undrained strength over the depth of

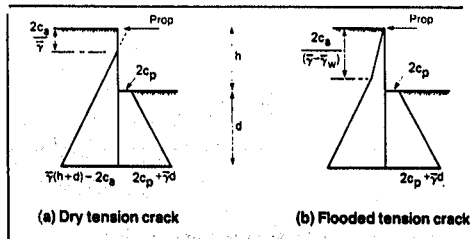

Fig. 4 Idealised stress distributions for the short-term analysis of walls propped at the crest.

embedment d on the excavated side would have forestalled failures of centrifuge models (Bolton and Powrie, 1987) and should equally enable preliminary assessments to be made of short term wall stability in practice.

Displacement on excavation

In addition to an assessment of the possibility of collapse, the designer will wish to ensure that the wall will not be rendered unserviceable by excessive deformations. Bolton and Powrie (1988) show that the shear strains induced in neighbouring soil zones by the deflections of a rigid, embedded wall can usefully be idealised as uniform. For example, the soil deformations associated with a wall rotating about its toe can be represented by triangular zones behind and in front of the wall, within which the shear strain γ is constant and equal to $2\delta/H$ as shown in ***Fig. 6.*** Although this simple relationship was derived for the case of a frictionless wall, data presented by Milligan and

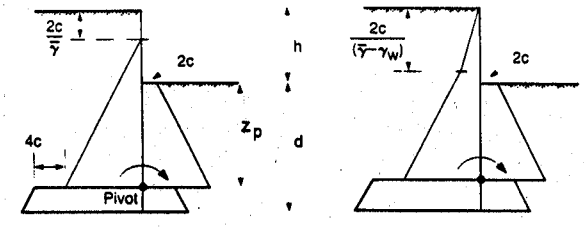

Fig. 2 Idealised stress distributions for the short-term analysis of unpropped cantilever walls.

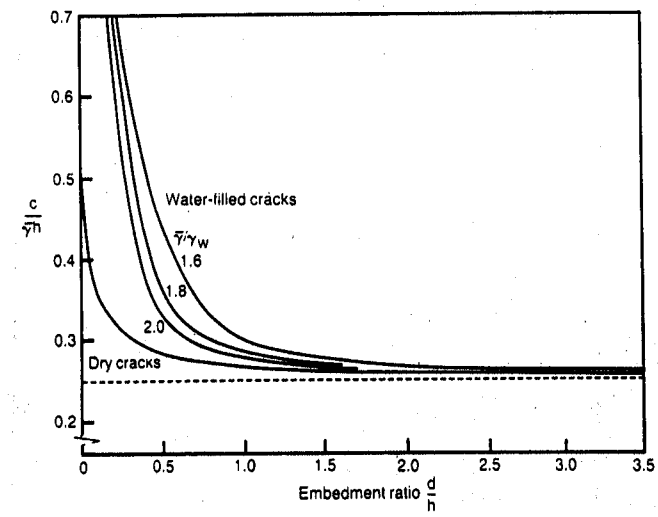

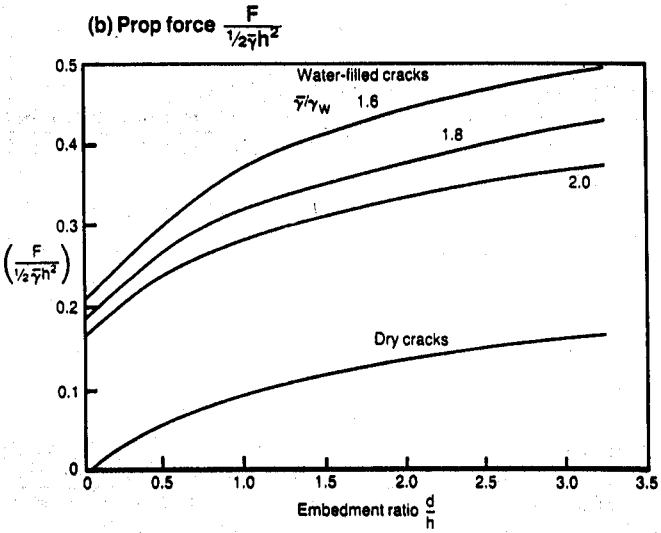

Fig. 5 LEFT: Mobilised shear strength $\left(\frac{c}{\bar{\gamma}h}\right)$ ***and prop force*** $\left(\frac{F}{\frac{1}{2}\bar{\gamma}h^2}\right)$ ***as a function of embedment ratio*** $\frac{d}{h}$ ***for walls propped at the crest.***

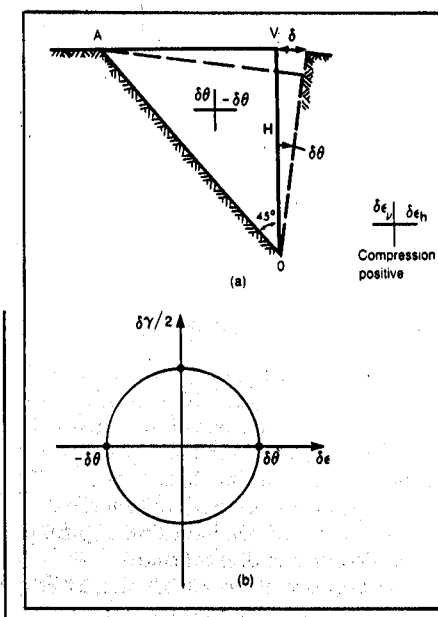

Fig. 6 RIGHT: Idealised strain field for a rigid bulkhead rotating about the toe.

Bransby (1976) indicate that it is also applicable, without significant error, to rough walls. The designer can aim to control wall displacement δ by limiting soil shear strains. A permissible displacement leads to a permissible soil strain which can then lead to the selection of a suitable mobilised soil strength, through laboratory test data presented as shown in ***Figure 7.***

It follows that the penetration ratio of a free cantilever wall which is required to limit the mobilisation of soil strength to c_{mob} is exactly that which has already been indicated in ***Figure 3,*** inserting c_{mob} in place of c_u in the stability number. Note the implication for a typical early stage of wall construction in which d/h = 1. If the wall is unpropped and subject to water-filled cracks then $c_{mob} \simeq 0.6\bar{\gamma}h$, whereas without water $c_{mob} \simeq 0.3\bar{\gamma}h$. For a typical 5m excavation stage in stiff clay with c_u = 100 kPa, this would offer mobilisation factors $\beta = c_{mob}/C_u$ between 0.3 and 0.6 which, taking the total wall height to be 10m, would generate wall movements of between 14mm and 90mm if the data shown in ***Figure 7*** were applicable. Clearly, the presence or otherwise of hydraulic thrust is a significant determinant of short-term wall behaviour.

Figure 8 compares the soil displacements computed in this way with those measured during a centrifuge test on an unpropped wall in which water-filled cracks were not observed. It may be seen that the two patterns of deformation are in good agreement. It seems likely that if sufficient penetration is included to prevent collapse in the presence of hydraulic thrust, and also to limit deformations to permissible values in the absence of hydraulic thrust, then there will be insufficient tensile strain to cause the soil to crack during construction.

A stiff wall propped rigidly at the crest would be expected to deflect by rotation about the crest: the corresponding idealised stress distributions, with and

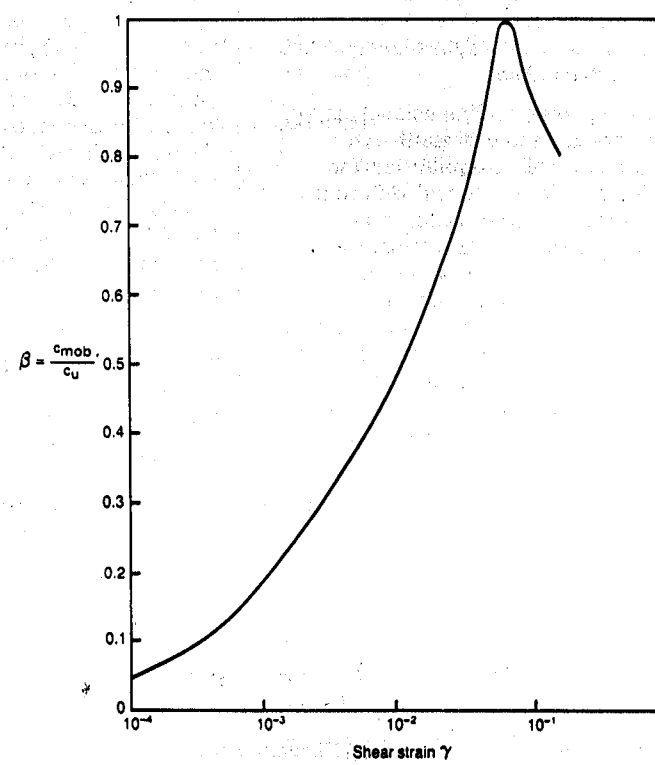

Fig. 7 Mobilised shear strength as a function of shear strain for a sample of London Clay tested in conventional undrained triaxial compression (original data from Jardine et al, 1984).

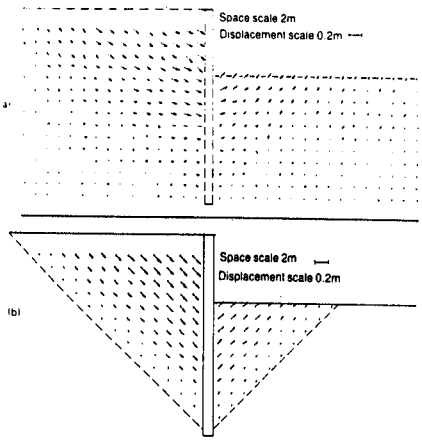

(a) Soil movements during excavation, test DWC08; (b) calculated displacements during excavation, test DWC08

Fig. 8 Comparison of measured and calculated soil displacements for a centrifuge model test on an unpropped wall with $\frac{d}{h} = 2$ (after Bolton and Powrie, 1988).

without water filling tension cracks, were shown in ***Figure 4.***

The kinematics are, however, more complex and the idealised deformation pattern must be assembled from simpler building blocks. ***Figure 6*** shows a set of admissible deformations compatible with a rigid bulkhead rotating outwards about the toe. For a similar inward rotation the signs of the strains are reversed but the magnitude of the maxiumum shear strain remains $2\delta/H = 2\vartheta$. ***Figure 9*** shows an idealised deformation pattern behind a rigid bulkhead rotating outward about the crest. In this case, it is necessary to imagine a square ABOV drawn in the soil. The upper triangle AOV rotates as a rigid body about V: the lower triangle AOB deforms in shear with uniform shear strain $2\delta/H = 2\vartheta$. Again, the signs of the strains are reversed for a corresponding inward rotation.

Figure 10 shows the idealised strain field for an embedded wall OUV rotating about the crest O. The strain field behind the wall corresponds exactly to ***Figure 9.*** In front of the wall, the horizontal movement at U is $h\vartheta$ and the horizontal movement at the toe V is $(h + d)\vartheta$ where h is the retained height, d is the embedment and ϑ is the rotation of the wall. Thus the strain field in front of the wall must be synthesised from components corresponding to an inward rotation about

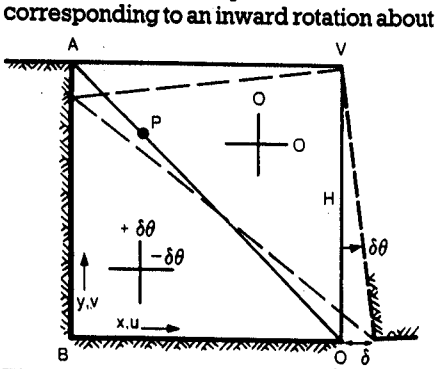

Fig. 9 Idealised strain field for a rigid bulkhead rotating about the crest.

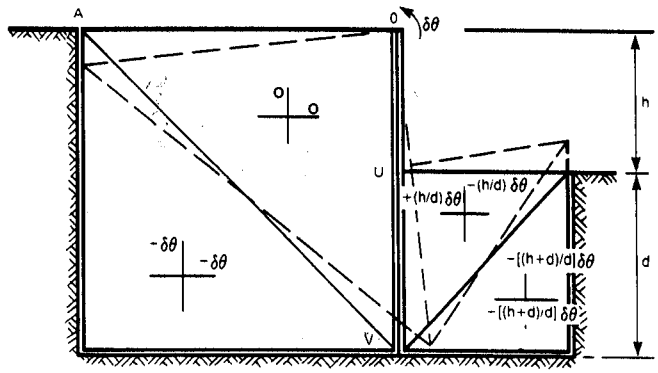

Fig. 10 Idealised strain field for an embedded wall rotating about the crest.

V of magnitude $h\vartheta/d$ ***(Fig. 6)*** superimposed on an inward rotation about U of $(h + d)\vartheta/d$ ***(Fig. 9).***

This means that the maximum shear strain in front of the wall is due to the second component and is of magnitude $2(1 + h/d)\vartheta$ – that is, $(1 + h/d)$ times the maximum shear strain on the retained side of the wall. An iterative method of solution should be employed so that the mobilised soil strength on the excavated side reflects these enhanced shear strains.

It should be recognised that this ratio simply characterises the maximum strains expected either side of the wall. Bolton and Powrie (1988) showed that the actual ground displacements in models were of a similar magnitude to those predicted, but that the settlement trough on the retained side spread beyond the point A in ***Fig. 10.*** As might have been expected there was no 'step' at that point. The data from the Bell Common Wall (Tedd et al, 1984) also show no such discontinuity.

Example calculation

Suppose a new road is to be constructed in a cut and cover tunnel where it passes through a designated conservation area. The side walls of the tunnel are to be constructed in situ using the diaphragm wall technique, and roof slab when placed will act as a prop. The proposed sequence of construction is:

- ☐ Installation of reinforced concrete diaphragm walls with ground level at OD
- ☐ excavation between the walls to −4m AOD
- ☐ installation of roof slab which acts as a prop at the crest of each wall
- ☐ excavation to −8m AOD with installation of sump drains to maintain the groundwater level between the walls at −9m AOD.

The wall is to be constructed in London Clay, and the idealised excavation geometry is shown in ***Figure 11.*** Note that the wall is assumed to be effectively rigid and the thickness of the wall is neglected, in that shear on the base is not included in the calculations. The problem facing the designer is the selection of a depth of embedment to ensure that the wall remains both stable and serviceable during temporary works activities and in the long term.

In this section, the temporary works activitities are investigated by using the methods described above to analyse an unpropped wall retaining 4m of London Clay. The stress-strain relationship (c_{mob}/c_u vs γ) which will be used in the analysis was shown in ***Fig. 7,*** being derived from the data of Jardine et al (1984) for an undrained triaxial test on an intact specimen of London Clay preconsolidated to 200kPa, which reached a peaked strength $c_u = 101$kPa. For the purpose of this calculation it will be assumed that these data adequately represent the stress-strain behaviour of the soil at all depths on both sides of the wall. For an undrained triaxial compression test, the volumetric strain $\varepsilon_{vol}(=\varepsilon_a + 2\varepsilon_r)$ is zero. Consideration of Mohr's circle of strain leads to the result that the maximum shear strain $\gamma(=\varepsilon_a - \varepsilon_r)$ is 1.5 times the axial strain ε_a.

Phase I: Wall unpropped, excavation to −4 m.

The wall will ultimately have to retain 8m of clay: suppose that its height H will have to be 20 m. Then for this phase h = 4m, d = 16 m.

Inserting d/h = 4 into ***Figure 3*** it is found that, without water in tension cracks:

$$c_{mob}/\bar{\gamma}h = 0.26$$

and taking $\bar{\gamma} = 20$ kN/m^3, gives:

$$c_{mob} = 0.26 \times 20 \times 4 = 21 \text{ kPa}$$

Note that the presence of water in tension cracks is immaterial here due to the overwhelming significance of the embedded length. With water in the crack $c_{mob} = 23$ kPa would be needed.

Taking a representative undrained shear strength to be $c_u = 100$ kPa gives

$$c_{mob}/c_u = 0.23$$

Inserting this ***Figure 7,*** the shear strain is found to be:

$$\gamma_1 = 1.5 \times 10^{-3}$$

Considering the 97.5% of the wall above the pivot point, the crest deflection δ_1 can then be deduced from:

$$\gamma_1 = \frac{2\delta_1}{0.975(h+d)}$$

which gives $\delta_1 = 15$mm.

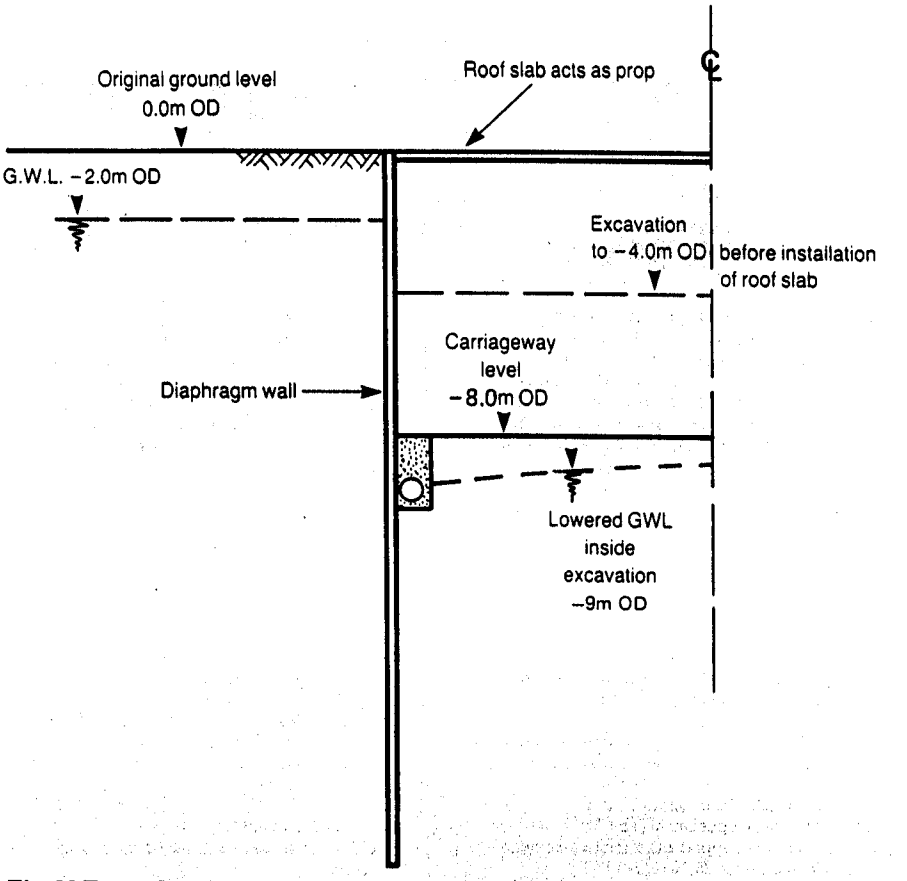

Fig. 11 Example calculation: definition of problem geometry.

Phase II: Wall propped at top, excavation to −8m

The penetration ratio will then be:
d/h= 12/8 = 1.5

As a preliminary estimate, assume the same mobilisation of strength everywhere. With dry tension cracks **Fig. 5** indicates for propped walls:

$$c_{mob}/\bar{\gamma}h = 0.26$$

so that

$$c_{mob} = 0.26 \times 20 \times 8 = 42\,kPa$$

This leads to a calculated mean mobilisation of strength

$$c_{mob}/c_u = 0.42$$

Figure 7 then indicates a mean shear strain after Phase II of:

$$\gamma_2 = 7.1 \times 10^{-3}$$

Since wall rotations about the toe (Phase I) and the crest (Phase II) have been idealised as causing maximum strains in different zones (upper and lower triangles, respectively) it will be convenient and conservative to treat the corresponding strains as independent. Accordingly, sufficient rotation about the crest to generate all of $\gamma_2 = 7.1 \times 10^{-3}$, is now allowed, ignoring the prior mobilisation of γ_1. Let the passive and active components be γ_{2p} and γ_{2a}: these should be in the ratio

$$\gamma_{2p} = (1 + h/d)\,\gamma_{2a} = 1.67\,\gamma_{2a}$$

As an approximation, therefore, take

$$(\gamma_{2p} + \gamma_{2a})/2 = 7.1 \times 10^{-3}$$

so that

$$\gamma_{2a} = 5.3 \times 10^{-3}, \gamma_{2p} = 8.8. \times 10^{-3}$$

Then, if δ_2 is the outward deflection of the toe during Phase II;

$$2\delta_2/20 = 5.3 \times 10^{-3}$$

so that

$$\delta_2 = 53mm.$$

This result is only approximate. ***Figure 7*** may be used to deduce the different mobilised strengths on the two sides of the wall: on inserting these values into a stress analysis after the fashion of ***Fig. 4,*** it will be found that the condition of moment equilibrium about the prop is not satisfied. The approximate result can be refined by altering the deflection iteratively until the conditions of moment equilibrium and shear strain ratio are satisfied simultaneously, but this leads to a rather small adjustment which can usually be ignored. The most significant judgement will always remain the selection of a representative stress-strain curve, scaled in the manner of ***Fig. 7.***

Finally, the prop force for equilibrium at the end of Phase II with d/h = 1.5 can be found from **Fig. 5b** to be, taking a dry tension crack,

$$F_2 = 0.12(0.5\bar{\gamma}h^2) = 77kN/m$$

Conclusions

1. Attention has been drawn to the advantages of calculating mobilised soil strengths which provide force and moment equilibrium for a retaining wall. These mobilised strengths depend only on the assumed shape of the lateral pressure diagram.
2. It has been shown that the calculation of mobilised strength in the temporary works condition can depend significantly on the possibility that free water can enter tension cracks. Even when stiff clays can properly be regarded as undrained, failure can occur due to the hydraulic thrust of water filling an opening crack behind a wall which is improperly supported.
3. It has also been shown that the influence of differences in shear strain between different zones of soil can be accounted for, especially in the case of a rigid wall propped at its crest when the mobilized 'passive' strains will exceed the 'active' strains.
4. It has been possible to estimate the undrained deflection of in-situ walls, either unpropped or propped near the top, taking them to be rigid. This provides the designer with a straightforward method of satisfying a serviceability criterion, using stress-strain data for the soil. The security of this calculation will be wholly dependent on the relevance of this data. Nevertheless, it is considered that this approach – even based on 'typical' previously published triaxial test data from well-conducted tests on similar soils – will provide the designer with a greater appreciation of the likely performance of the structure than would have been the case if a traditional 'factor of safety' had been applied.

Acknowledgements

The work described in this paper forms part of the programme of the Transport & Road Research Laboratory and the paper is published by permission of the Director.

The views expressed in this paper are not necessarily those of the Department of Transport. Extracts from the text may be reproduced, except for commercial purposes, provided the source is acknowledged.

References

Bolton, M D & Powrie, W (1987). Collapse of diaphragm walls retaining clay. Geotechnique 37, No 3, 335-353.

Bolton, M D & Powrie, W (1988). Behaviour of

diaphragm walls in clay prior to collapse. Geotechnique 38, No 2, 167-189.
Burland, J B, Simpson, B and St.John, H (1979). Movements around excavations in London Clay, Proc 7th Eur Conf Soil Mech, Brighton, 1, 13-29.
Burland, J B, Potts, D M & Walsh N M (1981). The overall stability of free and propped embedded cantilever retaining walls. Ground Engng. 14, No 5, 28-38.
Jardine, R J, Symes, M J & Burland, J B (1984). The measurement of soil stiffness in the triaxial apparatus. Geotechnique 34, No 3, 323-340.
Milligan, G W E & Bransby, P L (1976). Combined active and passive rotational failure of a retaining wall in sand. Geotechnique 26, No 3, 473-494.
Padfield, C J & Mair, R J (1984). Design of retaining walls embedded in stiff clay. Report 104, Construction Industry Research and Information Association.
Potts, D M & Fourie, A B (1984). The behaviour of a propped retaining wall: results of a numerical investigation. Geotechnique 34, No 3, 383-404.
Powrie, W (1985). Discussion on Fifth Geotechnique Symposium in Print. The performance of propped and cantilevered rigid walls. Geotechnique 35, No 4, 546-548.
Powrie, W (1986). The behaviour of diaphragm walls in clay. PhD dissertation, Cambridge University.
Rowe, P W (1952). Anchored sheet pile walls. Proc Inst Civ Engrs, Ptl, 1, 27-70.
Rowe, P W (1955). Sheet pile walls encastre at the anchorage. Proc Inst Civ Engrs, Ptl, 4, 70-87.
Simpson, B (1984). Computational analysis of flexible retaining walls. Proc Symp. Soil-Structure Interaction, Institution of Structural Engineers, London.
Skempton, A W (1961). Horizontal stresses in an overconsolidated Eocene clay. Proc 5th Int Conf Soil Mech, Paris, 1, 351-357.
Tedd, P, Chard, B M, Charles, J A & Symons, I F (1984). Behaviour of a propped embedded retaining wall in stiff clay at Bell Common tunnel. Geotechnique 34, 513-532.
Wood, L A (1979). LAWPILE: a program for the analysis of laterally loaded pile groups and propped sheetpile and diaphragm walls. Adv Engng. Soft 1, No 4, 176-186.
Wood, L A (1984). LAWWALL: analysis of cantilever and multi-braced sheetpile and diaphragm walls. User manual. London: SIA Computer Services.

List of Symbols Part I

c – undrained shear strength mobilised at wall equilibrium.
c_{mob} – undrained shear strength mobilised in triaxial test.
c_u – undrained shear strength.
d – depth of wall penetration below ground level on excavated side.
EI – wall bending stiffness.
F – prop force per unit length.
H – total height of wall = h + d.
h – retained height.
h_o – depth of tension crack.
K_a – active earth pressure coefficient.
K_o – initial in situ earth pressure coefficient at rest.
K_p – passive earth pressure ecoefficient.
m – rate of increase in soil stiffness with depth.
R – flexibility factor.
z – depth below a free soil surface.
z_p – depth to point of rotation below ground level on excavated side.
β – mobilisation factor – c_{mob}/c_u.
γ – shear strain.
$\bar{\gamma}$ – unit weight of soil.
γ_w – unit weight of water.
δ – wall displacement.
ε_a – axial strain in triaxial test.
ε_h – horizontal strain.
ε_r – radial strain in triaxial test.
ε_v – vertical strain
ε_{vol} – volumetric strain.
ϑ – angle of wall rotation.
σ_h – horizontal total stress.
σ'_h – horizontal effective stress.
σ_v – vertical total stress.
σ'_v – vertical effective stress.

Papers

The second part of this paper deals with the long-term behaviour of stiff in-situ walls retaining overconsolidated clay. The first part, which is concerned with short term stability and displacement appeared in the previous issue of *Ground Engineering.*

The design of stiff in-situ walls retaining overconsolidated clay: Part II, long term behaviour

by MD Bolton, W Powrie and IF Symons

Introduction

Part I of the paper considered the stability and displacement of an effectively rigid reinforced concrete wall, constructed in-situ in overconsolidated clay. In Part II calculations will be advanced to control the long term behaviour of such a wall. The validity of these calculations can be checked by using beam theory on the resulting bending moment diagram to compute the additional flexural displacements of the wall. The analysis will be useful only if these are smaller than the rigid body displacements. This was discussed in Part I where a soil/wall stiffness ratio R was defined, and the suggestion made that the approach outlined would be applicable for walls with R values less than 1000.

During the period immediately after excavation the stability of the wall may be assisted by the excess pore water suctions which result from the removal of total stress. In the long term, as steady state seepage conditions are approached, the dissipation of these pore water suctions will have a destabilising effect on the wall. The designer must therefore ensure that the retaining wall will not collapse or become unserviceable in the long term.

The correct approach to an assessment of the long term performance of a diaphragm wall in clay is an analysis which considers pore wate pressures and effective stresses separately. Fortunately the pore water pressures corresponding to steady state seepage round an impermeable wall in homogeneous soil are easily calculated, and a convenient approximation is to take the difference in excess head between the retained side and the excavated side as linearly distributed around the wall (Symons, 1983).

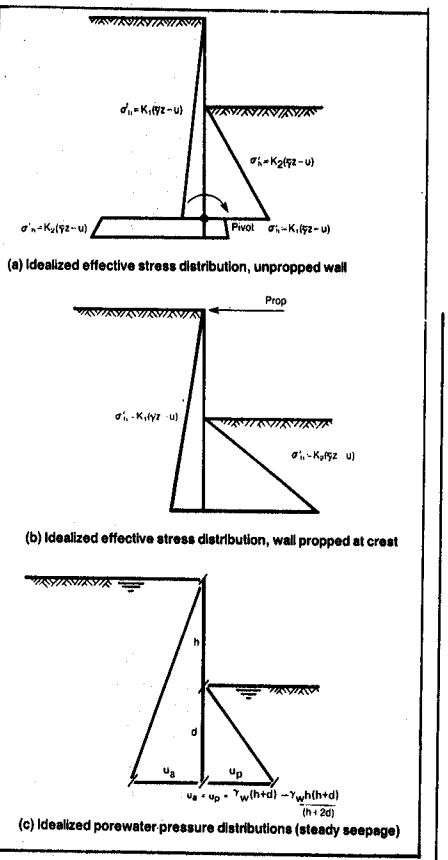

Figure 1: Idealised effective stress and porewater pressure distributions for the long term analysis of unpropped walls and walls propped at the crest.

The pore pressure distribution in the clay can, however, be greatly affected by inhomogeneities. A permeable silt or sand layer within the clay may, for example, be unaffected by the drawdown in the excavation, leading to fully hydrostatic conditions on the retained side above the layer, and enhanced hydraulic gradients for flow into the excavation. The homogeneous case will be considered hereafter for the purposes of explaining the proposed design method.

Stability

Idealised pressure distributions for stiff unpropped walls and walls propped rigidly at the crest are shown in ***Figure 1*** on the basis of a frictional limit condition. These are analagous to the stress distributions shown in Part I ***Figures 2 and 4*** for the cohesion analysis, but now the pore water pressures must be considered separately from effective stresses as indicated. In zones where the wall is moving away from the soil the lateral effective stress is given by $\sigma'_h = K_a(\bar{\gamma}z - u)$ where $(\bar{\gamma}z - u)$ is the vertical effective stress at a depth z below a free soil surface in the absence of wall friction. In zones

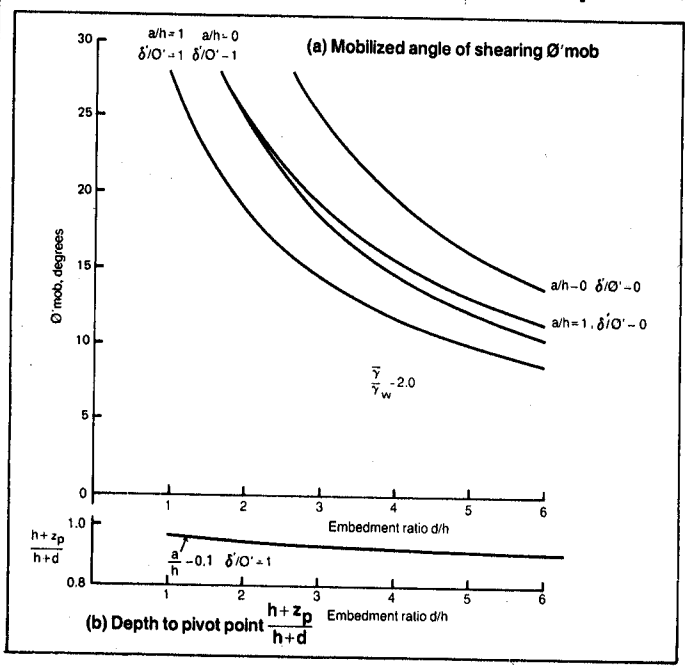

Figure 2: Mobilised angle of shearing ϕ_{mob} and depth to pivot $\frac{h+z_p}{h+d}$ as a function of the embedment ratio d/h for unpropped walls with uniform ϕ.

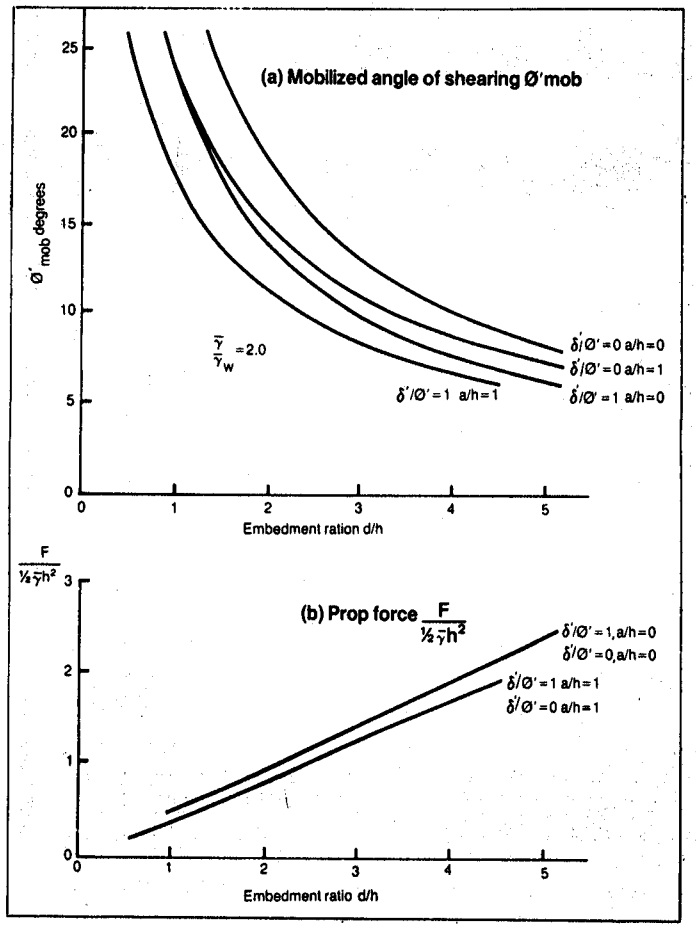

Figure 3: Mobilised angle of shearing resistance ϕ_{mob} and prop force $\frac{F}{\frac{1}{2}\bar{\gamma}h^2}$ as a function of embedment ratio d/h for walls propped at crest with uniform ϕ.

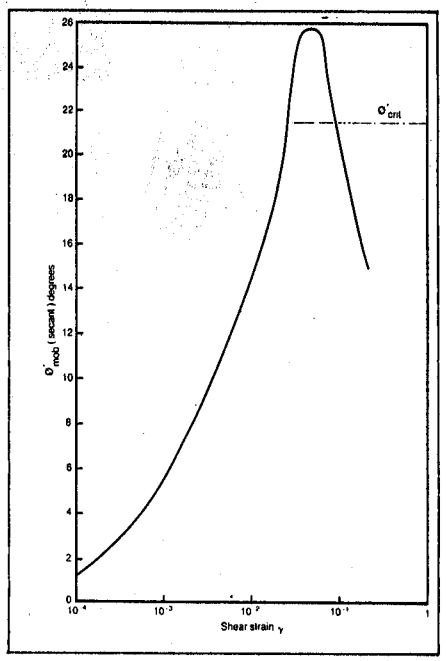

Figure 5: Mobilised angle of shearing resistance ϕ_{mob} as a function of shear strain γ for a sample of London clay in conventional undrained compression (original data from Jardine et al 1984).

where the wall is moving into the soil, $\sigma'_h = K_p(\bar{\gamma}z - u)$. The values of the earth pressure coefficients K_a and K_p might be evaluated so as to take account of the effects of wall friction using the methods of, for example, Caquot and Kerisel (1948) or Sokolovski (1960). Bolton and Powrie (1987) showed that the long-term collapse of stiff model walls in centrifuge tests was reliably predicted using this approach. Under working conditions, a reduced mobilised strength φ'_{mob} should be used to limit deflexions to an acceptable level. The idealised pressure distributions for a stiff unpropped wall are shown in ***Figure 1a.*** The equations of horizontal and rotational equilibrium are used, as before, to determine the two unknowns – the depth of the pivot point z_p and the mobilised angle of soil shearing φ'_{mob}, which is assumed to be uniform and equal on both sides of the wall.

Figure 2a plots the uniform angle of shearing φ' necessary to hold a stiff unpropped wall in equilibrium with a penetration ratio d/h, and with or without wall friction $\delta'/\delta' = 0$ or 1. Relations are given for the ratios of depth to phreatic surface on the retained side (a) to the retained height (h) of 0 and 1. As with the cohesion analysis, the pivot point was found to occur about 8% up the wall ***(Figure 2b)*** for the case $\bar{\gamma}/\gamma_w = 2.0$.

The idealised working pressure distributions for a stiff wall propped at the crest are shown in ***Figure 1b.*** Assuming that the angle of shearing resistance is the same everywhere, ***Figure 3a*** plots this value as a function of the embedment ratio d/h for $a/h = 0$ and 1, $\delta'/\varphi' = 0$ and 1, and $\bar{\gamma}/\gamma_w = 2.0$. ***Figure 3b*** gives values of $F/(\frac{1}{2}\bar{\gamma}.h^2)$ as a function of d/h where F is the prop force in kN per m run.

3. Deformation

As in Part I of the paper, the concept of mobilised soil strength can be used to assess the performance under working conditions of stiff walls which are either unpropped or propped near the crest. And although the constant-volume deformation mechanisms, used in ***Part I*** and repeated in ***Figure 4***, should not strictly apply where swelling will take place, they have been found to offer reasonable predictions of the long term

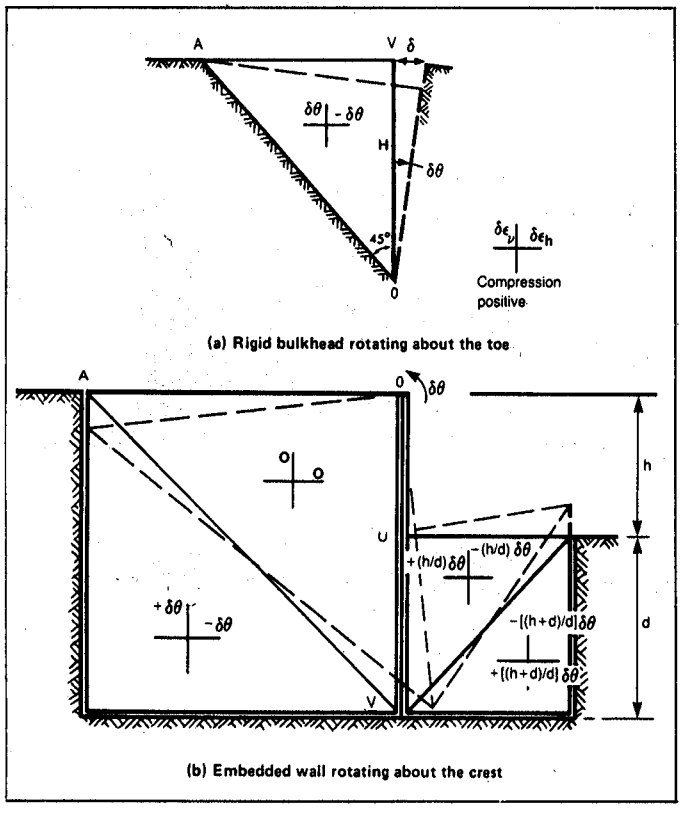

Figure 4: Idealised strain fields.

displacement of model walls in centrifuge tests (Bolton and Powrie, 1988).

For free cantilevers, ***Figure 4a*** may still be used to characterise soil deformations above the point of pivot, which is quite close to the toe of the wall (within about 8% of the total height).

In order to link shear strains with effective mobilised angles of soil shearing, data such as that shown in ***Figure 5*** will be required. Although there will be some variation with over consolidation ratio and test type – drained or undrained with pore pressure measurement, triaxial or plane strain – Powrie (1986) found that an undrained triaxial test carried out at the smallest likely OCR gave a conservative but reasonable lower bound. It is then possible to insert a trial geometry into ***Figure 2*** in order to deduce φ'_{mob} for equilibrium, insert this into constitutive data such as ***Figure 5*** to deduce shear strain γ, and to equate this to $2\delta/[0.92(h+d)]$ so that the crest deflection δ can be found.

Figure 4b can similarly be used to characterise deformations around a stiff wall propped at its crest. Initial guidance can then be obtained through the use of ***Figure 3*** to obtain an initial estimate of the mean mobilised soil strength φ'_{mob}. This can be inserted into ***Figure 5*** to obtain a mean shear strain γ. As before, the rate of increase of shear strain in the passive zone should be taken to be $(1+h/d)$ times that in the active zone leading to the earlier mobilisation of strength in the soil on the excavated side of the wall. A first estimate for the change in wall rotation $\Delta\vartheta$ would be:

$$2\Delta\vartheta = \Delta\gamma_a = 2\Delta\gamma_{av}/(2 + h/d)$$

so that

$$\Delta\vartheta = \Delta\gamma_{av}/(2 + h/d)$$

A more accurate assessment could be made through a careful appraisal of moment equilibrium about the prop, using earth pressure coefficients which correspond to the local mobilised soil strength φ'_{mob}, taken as a function of estimated shear strain in the zone concerned. In this way, variations with depth of wall friction, soil strength, soil stiffness, or pore pressure (arising from permeability variations) could also be allowed for. The simplest technique is to permit variation from the first estimate of wall rotation $\Delta\vartheta$, and to search for moment equilibrium using a micro-computer routine. Alternatively, but more laboriously, an iterative hand calculation will lead to the same result.

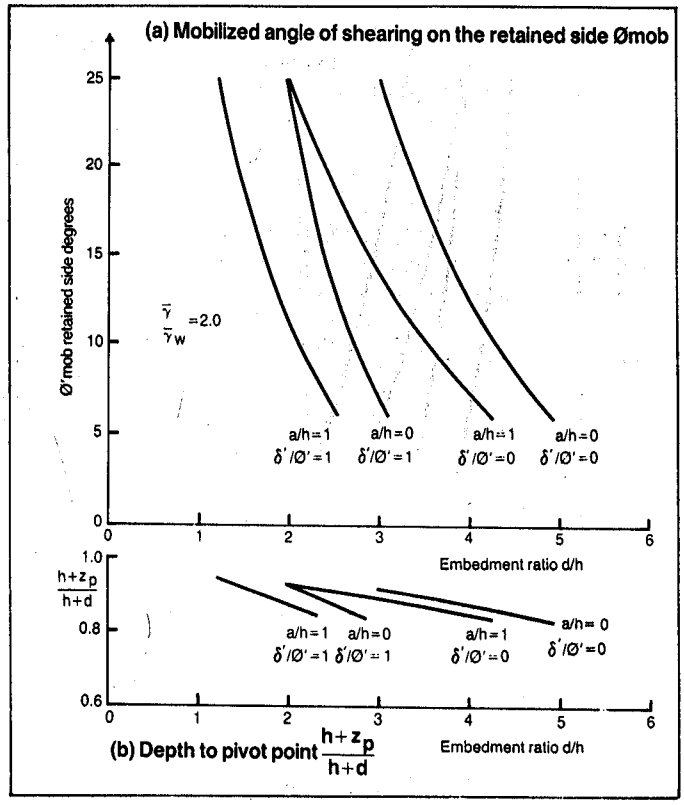

Figure 6: Mobilised angle of shearing ϕ_{mob} on the retained side and depth to pivot point $\frac{h+z_p}{h+d}$ as a function of embedment ratio d/h for unpropped walls with $\phi = 25°$ in front of the walls above the pivot.

The nature of the soil element tests which should ideally be carried out in order to generate the required stress-strain data has already been described in Part I. The measurement of pore water pressures during the test is necessary to obtain the constitutive relationship in terms of effective stress parameters (φ' versus γ). In the absence of appropriate stress path tests, the use of conventional triaxial compression test data should lead to a conservative result.

It can be shown, however, that for an overconsolidated clay, a significant depth of soil remaining in front of the wall below formation level will be brought to passive failure in the long term simply as a result of the removal of overburden during excavation. Under these circumstances it may be appropriate to assume that the soil in front of the wall mobilises a fully passive earth pressure coefficient irrespective of the strain. This considerably simplifies the calculation, since consideration of equilibrium leads to values of the earth pressure coefficient and hence the mobilised strength in the retained soil, and to the force exerted by the props and the bending moments induced in the wall. The rotation of the wall may then be estimated from stress/strain data representative of the behaviour of the retained soil only. The existence of earth pressure coefficients close to the passive limit in front of the wall, and in excess of the active limit behind the wall, is consistent with field studies (Carder and Symons, 1989) and finite element analyses (Potts and Burland, 1983).

Figure 6a plots the mobilised strength in the retained soil as a function of d/h for stiff unpropped walls, on the assumption that the strength mobilised in the soil above the pivot in front of the wall is 25°, for $\bar{\gamma}/\gamma_w = 2.0$, a/h = 0 and 1, and $\delta'/\varphi'_{mob} = 0$ and 1. ***Figure 6b***, which gives values of $(h + z_p)/(h + d)$, shows that there is, in this case, a rather more significant variation in the pivot position than previously: from 6% to 16% of the total height up from the base.

Figure 7a plots the mobilised strength in the retained soil, and ***Figure 7b*** the non dimensionalised prop force per unit length $F/(\frac{1}{2}\bar{\gamma}h^2)$, as a function of d/h for stiff walls propped at the crest on the assumption that the strength mobilised in the soil in front of the wall is 25°, again for a/h = 0 and 1, $\delta'/\varphi' = 0$ and 1, and $\bar{\gamma}/\gamma_w = 2.0$.

Example calculation

The methods described above will now be used to analyse the long term behaviour of the rigid wall first described in Part I with the geometry shown again in ***Figure 8.*** Note that the thickness of the wall is neglected, shear on the base is not included in the calculations. The constitutive relationship of ***Figure 5*** presented as a curve of mobilised angle of shearing φ_{mob} vs soil shear strain γ, will be used for this purpose. Phases I and II, detailed in Part I, concerned undrained soil behaviour during construction.

Phase III: Wall propped at the top, establishment of long term pore water pressures.

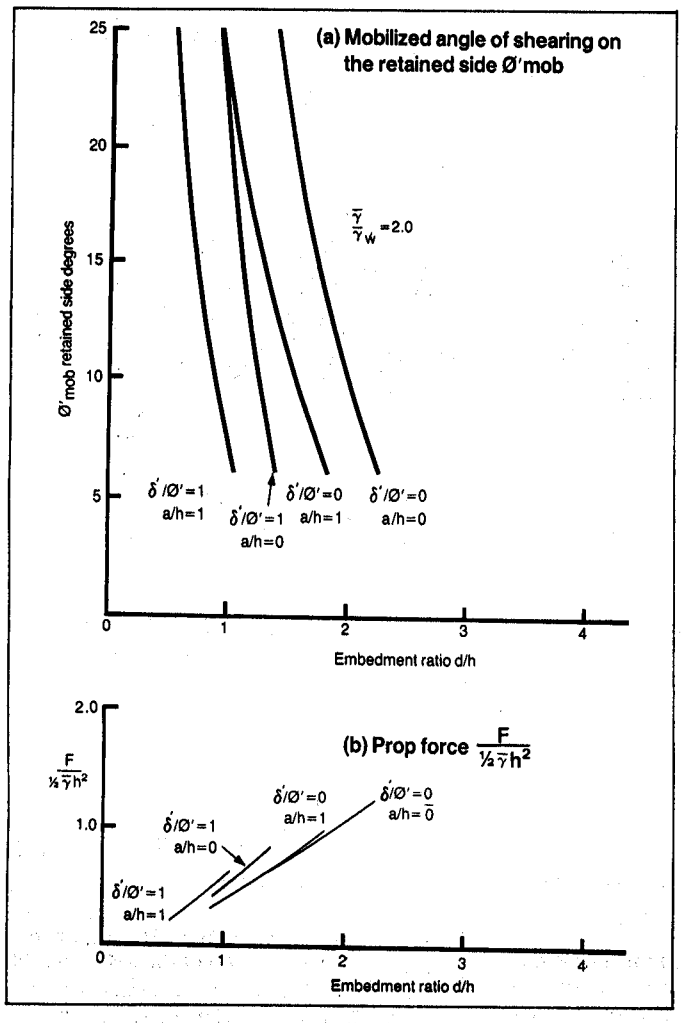

Figure 7: Mobilised angle of shearing resistance ϕ_{mob} on the retained side and prop force $\frac{F}{\frac{1}{2}\bar{\gamma}h^2}$ as a function of embedment ratio d/h for walls propped at crest with $\phi = 25°$ in front of the wall.

The wall has h = 8m and d = 12m so d/h = 1.5. The water table behind the wall is 2m below the retained soil surface, so a/h = 0.25.

Figures 2, 3, 6 and 7 have been calculated on the basis of a groundwater level in front of the wall at formation level, so their use in this case (with a slightly reduced groundwater level in front of the wall) should err on the conservative side. An angle of shearing can now be deduced which would just keep the wall in equilibrium if it were mobilised throughout. Inserting d/h = 1.5 into ***Figure 3a*** yields $\varphi' = 17.5°$ for a/h = 0 and $\delta'/\varphi = 1$, or $\varphi' = 13.7°$ for a/h = 1 and $\delta'/\varphi' = 1$. Linear interpolation between these values gives $\varphi'_{mob} = 16.6°$ for a/h = 0.25. Inserting $\varphi' = 16.6°$ into the stress-strain data of ***Figure 5*** yields $\gamma_3 = 15\times10^{-3}$m which can be treated as a mean mobilised shear strain.

Again, the shear strain increment on the excavated side of the wall should have been greater than that on the retained side by a factor of (1 + h/d) = 1.67, so that

$$\gamma_{3p} = 1.67\ \gamma_{3a}$$

As before, taking

$$(\gamma_{3p} + \gamma_{3a})/2 = 15\times10^{-3}$$

gives $\gamma_{3a} = 11.2\times10^{-3}$, $\gamma_{3p} = 18.8\times10^{-3}$

which is consistent according to ***Figure 5*** with mobilising strengths of about 15° on the retained side and 18° on the excavated side.

These results are approximate, because on performing an equilibrium check it will be found that there is a small out-of-balance resultant force acting on the wall. Neglecting this, the long-term horizontal displacement of the toe of the wall may be calculated from the rotation in Phase III following the installation of the prop:

$$\delta_3 = 20\vartheta_3 \text{ where } \vartheta_3 = \gamma_{3a}/2$$

$$\delta_3 = 20\times11.2\times10^{-3}/2 = 112\text{mm}$$

The outward movement of the wall at formation level is 8/20ths of this amount – that is, 45mm. This can be taken to be the total outward movement during Phases II and III, since the soil strains induced in Phase II can be considered as assisting in the mobilisation of strength in Phase III.

Alternatively, it might be assumed that the mobilised strength in the soil on the excavated side of the wall is 25° throughout due to passive swelling. Inspection of ***Figure 7*** shows that a wall with a penetration ratio d/h = 1.5 will ultimately mobilise φ' less than 5° on the retained side in these circumstances. Since this is actually less than was mobilised in the short term after Phases I and II, the additional movement in Phase III would clearly be negligible. The true state of the wall in the long term will lie between the two estimates based on zero volume change and full passive swelling.

The prop force F_3 may be calculated using ***Figure 3b*** assuming uniform mobilisation of φ':

$F_3 / (\frac{1}{2}\bar{\gamma}h^2) = 0.68$ for d/h = 1.5, $\delta'/\varphi' = 1$ and a/h = 0

$F_3/(\frac{1}{2}\bar{\gamma}h^2) = 0.56$ for d/h = 1.5, $\delta'/\varphi' = 1$ and a/h = 1

Interpolating, gives $F_3 / (\frac{1}{2}\bar{\gamma}h^2) = 0.65$ for $\delta'/\varphi' = 1$ and a/h = 0.25

Thus $F_3 = 0.65 \times 10 \times 8^2 = 416$kN/m run.

The additional refinement of satisfying strain compatibility leads to a very small modification, with F_3 = 421kN/m. However, the assumption of fully passive conditions with $\varphi' = 25°$ and $\delta'/\varphi' = 1$ beneath the excavation leads to a prop force F_3 = 612kN/m, which will be an upper bound to the true value if the passive earth pressure coefficient has been correctly inferred.

The maximum bending moments in the two extreme cases can easily be calculated from the lateral pressure diagrams. Neglecting swelling, and using the undrained triaxial compression data of ***Figure 5*** to achieve shear strain compatibility between the passive and active zones, the predicted bending moment would be 2360 kNm/m. In comparison, the bending moment with $\varphi'_{passive} = 25°$ beneath the excavation would be predicted to be 3350 kNm/m.

For design purposes, the "consistent shear strain" method will produce conservative over-estimates of rigid-body wall movements in the long term, while the "fully mobilised passive strength" method will produce conservative over-estimates of load effects induced in the structure.

Comparison with CIRIA report 104

The sensitivity of lateral stresses, prop forces and bending moments to the assumptions made in their calculation can be illustrated by considering the long-term behaviour of the rigid wall shown in ***Figure 8***. Design of the wall using the "worst credible scenario" approach given in CIRIA report 104, and assuming water levels at the ground surface on both sides, yields a required depth of embedment d = 10m. The assumed soil properties and angles of wall friction δ' are shown in ***Figure 9*** together with corresponding lumped factors of safety defined in various ways. Values of prop force and maximum bending moment have also been calculated and are listed in ***Table 1***. The

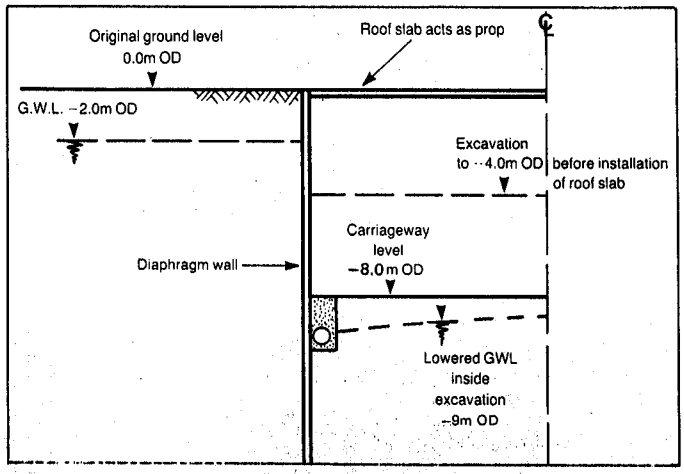

Figure 8: Example calculation: definition of problem geometry.

first row of values was derived in accordance with CIRIA report 104, assuming fully mobilised active and passive pressures acting over a reduced depth of embedment. The succeeding rows of values were derived using the methods proposed in this paper.

The initial 'uniform φ'_{mob}' approach is identical to using a 'factor of safety on soil strength', and the mobilised angle of shearing resistance can be expressed using $\tan(\varphi'_{mob}) = \tan(\varphi'_{max})/F_s$. For the case under consideration, moment equilibrium demands that $\varphi'_{mob} = 21°$. It will be seen from row 2 in ***Table 1*** that this assumption of a uniform mobilisation of strength leads to an increase in predicted load effects by about one third compared with the CIRIA method.

The third row of values in ***Table 1*** is derived from the 'consistent shear strain' refinement of the mobilised strength approach. Here it was necessary to make assumptions regarding initial soil stresses and stiffnesses. The effect of wall installation was taken to reduce the initial earth pressure coefficient to unity, and the relation between φ'_{mob} and shear strain was taken from ***Figure 5.*** An average shear strain of 24×10^{-3} was therefore deduced for $\varphi'_{mob} = 21°$. For strain compatibility the shear strain on the retained side γ_a would be 17×10^{-3} mobilising $\varphi'_{mob} = 17.5°$, and the shear strain on the excavated side would be 30×10^{-3} with $\varphi'_{mob} = 24°$, which is near to the peak value. If the iteration on mean strain, which would be necessary to satisfy both equilibrium and compatibility exactly, is neglected, a first order estimate of the horizontal displacement at the toe of the wall can be obtained using $\delta_h = (h+d)\,\gamma_a/2$ which gives 153mm. If that iteration is followed, it is found that $\gamma_a = 16 \times 10^{-3}$ with $\varphi'_{mob} = 17°$ on the retained side and $\gamma_p = 29 \times 10^{-3}$ with $\varphi'_{mob} = 23°$ on the excavated side, with a toe displacement of 144mm. The corresponding prop force and maximum bending moment are listed in row 3 of ***Table 1.***

To demonstrate the flexibility of the new approach, consider now the effect of assuming that the effective earth pressure coefficient after wall installation fell only to 1.5. This corresponds to an initial $\varphi'_{mob} = 11.5°$, in a passive sense, acting in the ground on both sides of the wall before excavation. Since the previous assumption of an earth pressure coefficient of unity after wall installation almost led to fully passive conditions beneath the excavation, it will now be taken that the prior bias towards passive conditions will guarantee their full achievement. Consideration of equilibrium then leads at once to the structural load effects listed in the fourth row of ***Table 1,*** and to the deduction $\varphi'_{mob} = 13.7°$ in an active sense on the retained side. From ***Figure 5*** this leads to a shear strain increment in the retained ground of approximately 14×10^{-3} and a corresponding toe displacement of about 126mm in the long term. A more careful assessment would, of course, require the collection of stress-strain data from appropriate load-unload-reload loops. It should be recognised that the effects of swelling beneath the excavation will similarly lead to the more rapid mobilisation of passive strength beneath the excavation: once it has been decided to permit full passive strengths to develop, the calculation set out above will apply.

It might, of course, be objected that there would be some uncertainty in the designation of fully passive pressures, should the engineer wish to invoke them. The final case considered in ***Table 1*** explores this sensitivity. Here the angle of wall friction is maximised, $\delta'/\varphi' = 1$, leading especially to larger passive pressure coefficients which are fully invoked beneath the excavation, and to the load effects listed in the fifth row of ***Table 1.*** The corresponding state on the retained side is $\varphi'_{mob} = 8.7°$, indicating an approximate shear strain of 7.7×10^{-3} and a toe deflection of about 70mm. It will be appreciated that structural load effects are now maximised while rigid body displacements are minimised. Only under these conditions would the projected wall movements be so small as not to warrant further concern: the projected bending moments are, however, 75% greater than those advocated in CIRIA report 104. It should be borne in mind that the use of upper bound soil strength parameters in determining fully passive pressures beneath excavation level means that no further enhancement factors need be applied to the resulting bending moments at equilibrium.

Table 1 **Comparison of design assumptions and methods**

Method (φ' values)	Prop Force kN/m	Maximum Bending Moment kN/m
CIRIA Report 104 (see figure 9)	280	1340
uniform φ'_{mob} ($\varphi'_{mob,a} = \varphi'_{mob,p} = 21°$)	360	1860
consistent shear strains ($\varphi'_{mob,a} = 17°$, $\varphi'_{mob,p} = 23°$)	390	2010
fully passive beneath excavation ($\varphi'_{mob,a} = 14°$, $\varphi'_{mob,p} = 25°$)	420	2140
fully passive beneath excavation full wall friction ($\delta'/\varphi'_{mob} = 1$) ($\varphi'_{mob,a} = 9°$, $\varphi'_{mob,p} = 25°$)	460	2350

Future groundwater conditions

There is currently some concern over the possible consequences of groundwater pressures rising in clays, especially in urban areas where the reduction of industrial activity has led to a decrease in water abstraction from deep aquifers. In the context of in situ retaining walls the raising of water levels might lead to increased lateral pressures in the retained clay. This increase would arise from the combined effects of an increase in pore water pressure and an increase in the effective earth pressure coefficient following swelling. If the structural system were very stiff, these increased stresses would create increased bending moments and propping forces. If the structural system were more flexible, the additional stresses might be relieved by further

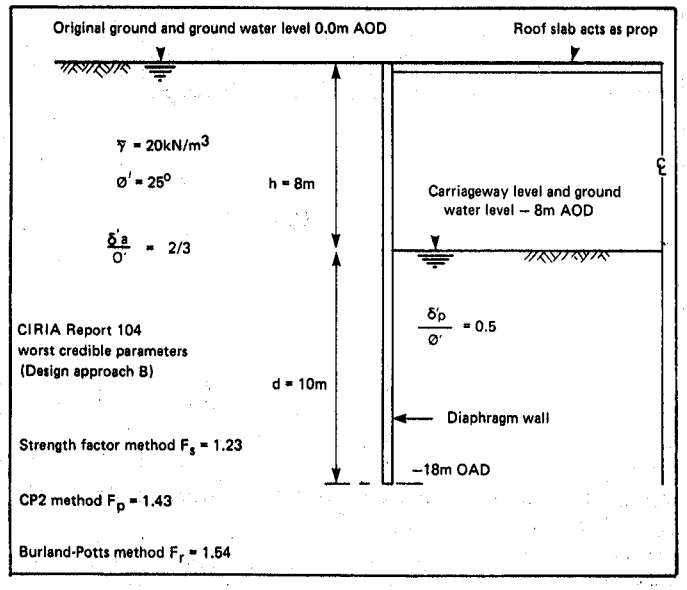

Figure 9: Example calculation: assumed properties and calculated factors of safety.

deflection of the wall. There is therefore a risk of a serviceability failure in which either the strength or the displacement criterion is violated. Both classes of behaviour are described in more detail by Bolton, Powrie and Stewart (1987).

Provided that the pore water pressures can be estimated, there seems no reason why the mobilised strength approach in terms of effective stresses should not be used to analyse the response of the wall to future changes in groundwater conditions. Back-analyses of a centrifuge test modelling an unpropped prototype wall of 10m retained height and 20m embedment with a rising ground water level tended to overpredict bending moments: this would suggest that if the mobilised strength approach is erroneous under such circumstances, it is at least conservative. The effects on propped walls are currently being studied in greater detail.

Where effective stresses are changing significantly as a result of a global rise in groundwater levels, the effects of volumetric strains on soil deformations cannot be ignored. A first order correction for volumetric strains would be to superimpose one-dimensional swelling effects on to the shear deformations predicted using the admissible strain fields of ***Figure 4.*** A more thorough approach would involve the careful selection of a swelling strain path in a triaxial test, Burland and Fourie (1985), from which effective stresses during swelling could be measured. Consistent shear and volumetric strains could then be invoked with stresses satisfying overall equilibrium of the wall in the general fashion set out above.

Conclusions

1. The advantages of calculating the mean mobilised angle of shearing resistance which, when applied uniformly in a Rankine-style stress analysis, provides force and moment equilibrium for a stiff retaining wall, have been demonstrated.
2. In the long term, clay soils drain and change their void ratio. Their strength criterion is then best expressed in terms of a secant angle of shearing resistance φ' based on effective stresses. It has been shown that the use of undrained triaxial tests with pore pressure measurement provides data of the mobilisation of φ' with shear strain which can be used to estimate drained soil deformations. The neglect of swelling beneath the excavation leads to an under-estimate of long term "passive" earth pressures and thereby to an upper bound estimate of the rotation of a rigid wall and a lower bound estimate of load effects in the structure. The possible influence of a fully passive condition due to long-term swelling beneath the excavation has also been demonstrated: this leads to a lower bound prediction for long-term wall rotations, but an upper bound estimate of structural load effects, assuming that the fully passive earth pressure coefficient can be determined.
3. The use of full-depth triangular earth pressure distributions with partially mobilised strengths, rather than the curtailed distributions of fully mobilised strengths advocated in CIRIA Report 104, leads to much larger predictions of long-term bending moments, consistent with measurements in model tests on relatively stiff walls. Furthermore, walls proportioned according to the CIRIA guidelines must apparently rely on the prior acquisition of passive conditions beneath the excavation if they are not to displace significantly.

Acknowledgements

The work described in this paper forms part of the programme of the Transport & Road Research Laboratory and the paper is published by permission of the Director.

The views expressed in this paper are not necessarily those of the Department of Transport. Extracts from the text may be reproduced except for commercial purposes, provided the source is acknowledged.

List of Symbols Part II

a – depth to phreatic surface below ground level on retained side.
d – depth of wall penetration below ground level on excavated side.
F – prop force per unit length.
F_p – factor of safety by Code of Practice method.
F_r – factor of safety by Burland-Potts method.
F_s – factor of safety by strength method.
h – retained height.
H – total height of wall = h + d.
K_a – active earth pressure coefficient.
K_o – initial in situ coefficient of earth pressure at rest.
K_p – passive earth pressure coefficient.
K_1 – mobilised active earth pressure coefficient.
K_2 – mobilised passive earth pressure coefficient.
u – porewater pressure.
z – depth below a free soil surface.
z_p – depth to point of rotation below ground level on excavated side.
γ – shear strain.
$\bar{\gamma}$ – unit weight of soil.
γ_w – unit weight of water.
δ – wall displacement.
δ' – angle of wall friction.
ϑ – angle of wall rotation.
σ'_h – horizontal effective stress.
$\sigma'v$ – vertical effective stress.
φ' – angle of shearing resistance.
φ'_{crit} – critical state of shearing resistance.
φ'_{mob} – mobilised angle of shearing resistance.

References

1. Bolton, M.D. & Powrie, W.(1987). Collapse of diaphragm walls retaining clay. Geotechnique 37, No 3, 335-353.
Bolton, M.D. & Powrie, W. (1987). Collapse of diaphragm walls retaining clay. Geotechnique 37, No 3, 335-353.
Bolton, M.D. & Powrie, W. (1988). Behaviour of diaphragm walls in clay prior to collapse. Geotechnique 38, No 2, 167-189.
Bolton, M.D., Powrie, W. & Stewart, D.I. (1987). Effects on diaphragm walls of groundwater pressure rising in clays. Proc 9th Eur Conf. Soil Mech. Fdn Engng 2, 759-762.
Burland, J.B. & Fourie, A.B. (1985). The testing of soils under conditions of passive stress relief. Geotechnique 35, No 2, 193-198.
Caquot, A. & Kerisel, J. (1948). Tables for the calculation of passive pressure, etc. Paris: Gauthier-Villars.
Carder, D.R. & Symons, I.F. (1989). Long-term performance of an embedded cantilever retaining wall in stiff clay. Geotechnique 39, No. 1, 55-75.
Jardine, R.J., Symes, M.J. & Burland, J.B. (1984). The measurement of soil stiffness in the triaxial apparatus. Geotechnique 34, No 3, 323-340.
Padfield, C.J. & Mair, R.J. (1984). Design of retaining walls embedded in stiff clay. Report 104, Construction Industry Research & Information Association.
Potts, D.M. & Burland J.B. (1983). A numerical investigation of the retaining walls of the Bell Common Tunnel, Suppl. Report 783, TRRL.
Powrie, W. (1986). The behaviour of diaphragm walls in clay. PhD dissertation, Cambridge University.
Sokolovski, V.V. (1960). Statics of soil media (tr. D.M. Jones & A.N. Schofield). London: Butterworths.
Symons, I.F. (1983). Assessing the stability of a propped insitu retaining wall in overconsolidated clay. Proc. Instn. Civ. Engrs., Pt2, 75, 617-633.